Easy-aligned off-axis three-mirror system with wide field of view using freeform surface based on integration of primary and tertiary mirror

Qingyu Meng,* Wei Wang, Hongcai Ma, and Jihong Dong

Changchun Institute of Optics, Fine Mechanics and Physics, Chinese Academy of Sciences, No. 3888, Dongnanhu Road, Changchun 130033, China

*Corresponding author: mengqy@ciomp.ac.cn

Received 14 January 2014; revised 1 April 2014; accepted 1 April 2014; posted 3 April 2014 (Doc. ID 204753); published 7 May 2014

An off-axis three-mirror system (OTS) was designed based on the primary mirror and tertiary mirror (TM) integrated on a single substrate in order to solve the OTS drawbacks, such as the alignment difficulty and the large opto-mechanical weight. Furthermore, an optical freeform surface that can increase the optimizing degrees of freedom (DOF) was applied on the TM in order to achieve a wide field of view (FOV). An example with a focal length of 1200 mm, F-number of 12, and FOV of 10° × 4° was given, and the maximum wave front error (WFE) RMS was 0.0126λ, indicating a good imaging quality. The design result shows that the number of alignment DOF was reduced from 12 to 6, and the weight of the mirror support assembly can also be lighter. An XY polynomial, established as an even function of x, was employed as the TM surface, so we obtained an axial symmetrical imaging quality about the x axis, and the axial symmetry aberration performance also brings considerable convenience to alignment and testing for the OTS.

OCIS codes: (080.3620) Lens system design; (080.1010) Aberrations (global); (120.3620) Lens system design; (220.3620) Lens system design.

http://dx.doi.org/10.1364/AO.53.003028

1. Introduction

With the rapid development of remote sensing, the design goal of the optical system moves toward high resolution and wide field of view (FOV). The off-axis three-mirror system (OTS) [1–4], which evolved from a coaxial three-mirror system, has been getting more attention since the discovery of the advantages of much wider FOV [5] and nonobscuration, which makes a better spot diagram energy concentration [6]. Both Korsch and Cook have introduced design forms that have no pupil obscuration [7], [8].

However, there are also drawbacks to OTS, such as alignment difficulty, high cost [9], [10], and large optomechanical weight. Therefore, to solve these problems, it is an essential way to design and optimize the optical system from basic theory. It can be easily found that, on many occasions, the axial positions of the primary mirror (PM) and tertiary mirror (TM) are close enough so that we hope the PM and TM can be integrated as a monolithic mirror through a proper design. Consequently, the alignment difficulty will be reduced to a great extent owing to the fewer degrees of freedom (DOF). Moreover, the weight of the mirror support assembly will also be lighter.

Furthermore, due to the finite optimization variables, achieving a very wide FOV of OTS is still beset with difficulties. So increasing the quantity of DOF of optimization variables is an effective way to achieve wide FOV. A simple solution to this problem is to introduce mirror position DOFs during the design process, such as mirror tilt variables, mirror decenter variables, image plane tilt variable, and so on, but it results in the alignment difficulty worsening in another way that we don't want to confront. Freeform

1559-128X/14/143028-07$15.00/0

surfaces are a category of nonrotational symmetric surfaces that have strong abilities of aberration correction since they obtain multiple DOFs compared with conventional optical surfaces. Now the optical freeform surface manufacturing technology is becoming more and more mature, and the optical freeform surface has been successfully applied in illumination systems and imaging systems [11–15]. The freeform surface can increase the DOF of surface shape, which makes realization of imaging system with a wide FOV possible.

In this paper, we design an easy alignment OTS by using an optical freeform surface based on integration of PM and TM, which can not only achieve a very wide FOV but also reduce the alignment difficulty. The system has very good application prospects in the optical remote sensing field.

2. Design Principle and Establishing Initial Configuration Based on Third Order Aberration

In order to achieve the integration of the PM and TM, theoretically speaking, they should have as many of the same parameters as possible. A similar profile will lower the fabrication difficulty and hence ensure the fabrication accuracy. At least three basic requirements should be satisfied. First, the axial position of the PM and TM should be equal. Second, they should have the same radius of curvature or mirrors with a different radius of curvature will hardly be fabricated on a single substrate. Third, they should have the same conical coefficient, i.e., $k_1 = k_3$, which will lower the grinding difficulty.

What should be emphasized is that the optical system that we want to achieve has no decenter in PM and TM, so the PM and TM have the same optical axis. And it will reduce the cost and processing time at initial stage of mirror finishing if we set the radius of curvature and conical coefficient of PM equal to TMs, because the optical spherical surface of PM and TM could be grinded simultaneously. Then, the different surfaces can be lapped and polished respectively in the region of themselves. It should be mentioned that the computer generated holography (CGH) could be used in PM and TM testing.

OTS derives from a coaxial three-mirror system [16]. Generally, an OTS begins with solving the initial structure of a coaxial three-mirror system, which is shown in Fig. 1. M1, M2, and M3 are the PM, secondary mirror (SM), and TM. $-l'_1$ is the focal length of the PM, l_2, l'_2, l_3, l'_3 are the object distance of SM, image distance of SM, object distance of TM, and image distance of TM, respectively. h_1, h_2, h_3 are the diameters of PM, SM, and TM, respectively, u_2, u'_2 are the object aperture angle and image aperture angle of PM, respectively, u_3, u'_3 are the object aperture angle and image aperture angle of SM, respectively [17].

In the system, there are four variables, $\alpha_1, \alpha_2, \beta_1, \beta_2$, which are PM obscuration ratio caused by SM, SM obscuration ratio caused by TM, SM magnification, and TM magnification, respectively; they can express all of the concerned parameters, including

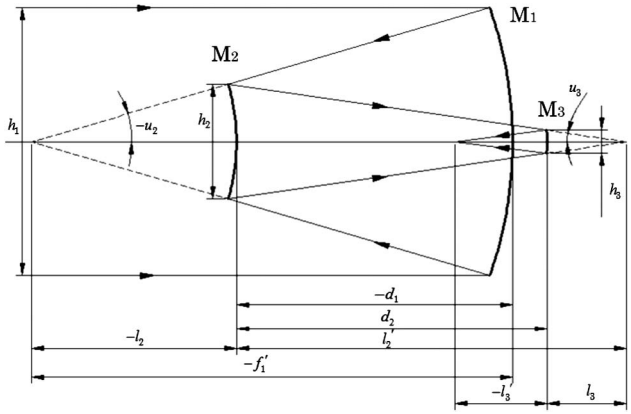

Fig. 1. Initial configuration of coaxial three mirrors.

the original profile and third-order aberration coefficients:

$$\alpha_1 = \frac{l_2}{l'_1} = \frac{h_2}{h_1}, \tag{1}$$

$$\alpha_2 = \frac{l_3}{l'_2} = \frac{h_3}{h_2}, \tag{2}$$

$$\beta_1 = \frac{l'_2}{l_2} = \frac{u_2}{u'_2}, \tag{3}$$

$$\beta_2 = \frac{l'_3}{l_3} = \frac{u_3}{u'_3}. \tag{4}$$

The normalized profile parameters (normalized respect the system focal length) of the initial structure can be expressed based on paraxial optical theory: r_1, r_2, r_3, d_1, d_2 are the PM radii of curvature, SM radius of curvature, TM radius of curvature, distance between PM and SM, and distance between SM and TM, respectively:

$$r_1 = \frac{2}{\beta_1\beta_2}, \tag{5}$$

$$r_2 = \frac{2\alpha_1}{(1+\beta_1)\beta_2}, \tag{6}$$

$$r_3 = \frac{2\alpha_1\alpha_2}{1+\beta_2}, \tag{7}$$

$$d_1 = \frac{1-\alpha_1}{\beta_1\beta_2}, \tag{8}$$

$$d_2 = \frac{\alpha_1(1-\alpha_2)}{\beta_2}. \tag{9}$$

Following Eqs. (5)–(9), r_1, r_2, r_3, d_1, d_2 are directly expressed by $\alpha_1, \alpha_2, \beta_1, \beta_2$, which means, from a set of $\alpha_1, \alpha_2, \beta_1, \beta_2$, these structure parameters can be determined uniquely.

In the three-mirror system, there are relationships between third order aberration coefficients, that is,

Seidel spherical aberration coefficient S_{I}, Seidel coma aberration coefficient S_{II}, Seidel astigmatism aberration coefficient S_{III}, and the design variables $\alpha_1, \alpha_2, \beta_1, \beta_2$:

$$S_{\mathrm{I}} = \frac{1}{4}\Big[(-k_1-1)\beta_1^3\beta_2^3 + k_2\alpha_1\beta_2^3(1+\beta_1)^3 - k_3\alpha_1\alpha_2(1+\beta_2)^3 + \alpha_1\beta_2^3(1+\beta_1)(1-\beta_1)^2 - \alpha_1\alpha_2(1+\beta_2)(1-\beta_2)^2\Big], \quad (10)$$

$$S_{\mathrm{II}} = \frac{k_2(\alpha_1-1)\beta_2^3(1+\beta_1)^3}{4\beta_1\beta_2} - \frac{k_3[\alpha_2(\alpha_1-1)+\beta_1(1-\alpha_2)]}{4\beta_1\beta_2} \cdot (1+\beta_2)^3 + \frac{(\alpha_1-1)\beta_2^3(1+\beta_1)(1-\beta_1)^2}{4\beta_1\beta_2} - \frac{[\alpha_2(\alpha_1-1)+\beta_1(1-\alpha_2)](1+\beta_2)(1-\beta_2)^2}{4\beta_1\beta_2} - \frac{1}{2}, \quad (11)$$

$$S_{\mathrm{III}} = \frac{k_2\beta_2(\alpha_1-1)^2(1+\beta_1)^3}{4\alpha_1\beta_1^2} - \frac{k_3[\alpha_2(\alpha_1-1)+\beta_1(1-\alpha_2)]^2}{4\alpha_1\alpha_2\beta_1^2\beta_1^2} \cdot (1+\beta_2)^3 + \frac{\beta_2(\alpha_1-1)^2(1+\beta_1)(1-\beta_1)^2}{4\alpha_1\beta_1^2} - \frac{1}{4\alpha_1\alpha_2\beta_1^2\beta_1^2} \cdot [\alpha_2(\alpha_1-1)+\beta_1(1-\alpha_2)]^2(1+\beta_2)(1-\beta_2)^2 - \frac{1}{\alpha_1\beta_1} \cdot \beta_2(\alpha_1-1)(1+\beta_1)(1-\beta_1) - \frac{[\alpha_2(\alpha_1-1)+\beta_1(1-\alpha_2)]}{\alpha_1\alpha_2\beta_1\beta_2} \cdot (1+\beta_2)(1-\beta_2) - \beta_1\beta_2 + \frac{\beta_2(1+\beta_1)}{\alpha_1} - \frac{1+\beta_2}{\alpha_1\alpha_2}. \quad (12)$$

The relationship between aberration coefficient and $\alpha_1, \alpha_2, \beta_1, \beta_2$ can be expressed by a set of equations:

$$\begin{bmatrix} S_{\mathrm{I}} \\ S_{\mathrm{II}} \\ S_{\mathrm{III}} \end{bmatrix} = \begin{bmatrix} A_1(\beta_1,\beta_2) & B_1(\beta_1,\beta_2) & C_1(\alpha_1,\alpha_2,\beta_2) \\ A_2(0) & B_2(\alpha_1,\beta_1,\beta_2) & C_2(\alpha_1,\alpha_2,\beta_1,\beta_2) \\ A_3(0) & B_3(\alpha_1,\beta_1,\beta_2) & C_3(\alpha_1,\alpha_2,\beta_1,\beta_2) \end{bmatrix} \times \begin{bmatrix} -k_1 \\ -k_2 \\ -k_3 \end{bmatrix} + \begin{bmatrix} D_1(\alpha_1,\alpha_2,\beta_1,\beta_2) \\ D_2(\alpha_1,\alpha_2,\beta_1,\beta_2) \\ D_3(\alpha_1,\alpha_2,\beta_1,\beta_2) \end{bmatrix}, \quad (13)$$

where k_1, k_2 and k_3 denote the conic of PM, SM, and TM. A_i, B_i, C_i, D_i $(i = 1, 2, 3)$ are functions of $\alpha_1, \alpha_2, \beta_1, \beta_2$.

In order to achieve the goal of integrating the PM and TM,

(1) the PM and TM have the same axial position, $d_1 = -d_2$;
(2) the PM and TM have the same radius of curvature, $r_1 = r_3$;
(3) the PM and TM have the same conical coefficient, $k_1 = k_3$;
(4) the aberration coefficients are equal to 0.

Noting that we let $k_1 = k_3$, generally, there must be $S_{\mathrm{I}} \neq S_{\mathrm{III}}$. Considering that spherical aberration is on-axis aberration and easily corrected, S_{III} is set to 0. Therefore, given the original α_1 and α_2, the other parameters $\beta_1, \beta_2, k_1, k_2$ can be derived from these equations. The relationships between α and β are

$$\beta_1 = \frac{1-\alpha_1}{\alpha_1(\alpha_2-1)}, \quad (14)$$

$$\beta_2 = \frac{\alpha_2-1}{1-\alpha_1\alpha_2}. \quad (15)$$

From the above analysis, we can obtain a set of original structure parameters, including curvature radius of PM, SM (the TM's curvature radius is equal to PM's), distance between PM and SM (distance between SM and TM is equal to the absolute value PM and SM), and conic constant k_1 and k_2 (the value of k_3 is equal to k_1).

In this system, the PM and TM have the same axial position, radius of curvature and conic, and hence they can be integrated as a monolithic mirror in the fabrication and alignment. This is a fine condition in which we can achieve the design goal; the OTS's PM and TM could be integrated on a single substrate. The residual aberrations can be corrected by kinds of optimizing methods, such as optimizing surface shape parameters, changing the off-axis amount, adding the higher-order aspherical term, and so on. This optimizing process can be achieved with the optical design software CODE V and Zemax via establishing merit function, setting optimizing boundary condition after the initial configuration is given.

3. Analysis and Application of Optical Freeform Surface

Based on the analysis of the previous section, the initial configuration of the OTS whose PM and TM can be integrated on a single substrate was obtained. However, the off-axis aberration is still difficult to correct, because there is very limited design DOF, especially when we add many more restrictions on the parameters of PM and TM. So increasing design DOFs by other methods is an essential and effective way to achieve a wide FOV of.

Freeform surfaces are a category of nonrotational symmetric surfaces that have strong ability in aberration correction due to multi-DOFs compared with conventional optical surfaces. It has begun to be widely used in illumination systems and imaging systems since the development of manufacturing technology.

Zernike polynomial surfaces and XY polynomial surfaces are two common optical freeform surfaces.

The Zernike surface is defined by the conical surface plus additional aspheric terms defined by the Zernike coefficients, while these terms directly

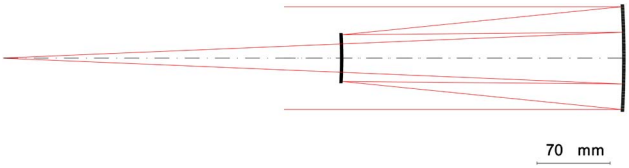

Fig. 2. Initial configuration.

correspond to the geometric aberration coefficients [18]. The surface sag is of the form

$$z = \frac{cr^2}{1+\sqrt{1-(1+k)c^2r^2}} + \sum_{i=1}^{N} A_i Z_i(\rho,\varphi), \qquad (16)$$

where c is the curvature (the reciprocal of the radius), r is the radial coordinate in lens units, k is the conic constant, ρ is the normalized radial ray coordinate, and φ is the angular ray coordinate. N is the number of Zernike coefficients in the series. A_i is the coefficient on the ith Zernike standard polynomial, and its unit is millimeter.

The XY polynomial surface supports a basic conic aspheric surface upon which the polynomial aspheric terms are added. Combining the XY polynomial and optical system coordinate, x represents the sagittal direction of the optical system and y represents the tangential direction. The surface sag is of the form

$$z = \frac{cr^2}{1+\sqrt{1-(1+k)c^2r^2}} + \sum_{i=1}^{N} A_i E_i(x,y), \qquad (17)$$

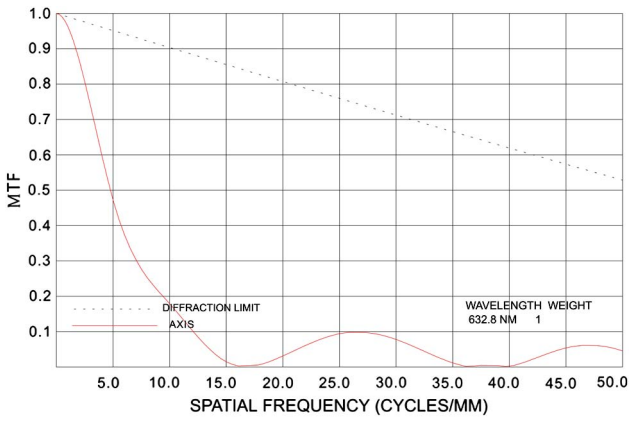

Fig. 3. MTF of initial configuration.

where N is the number of polynomial coefficients in the series and A_i is the coefficient on the ith XY polynomial, and its unit is millimeter.

The polynomials are a power series in x and y.

Compared to the Zernike polynomial, XY polynomial surfaces are easier to process due to the consistence with the numerical control (NC) optical expression form, although the aberrations are not explicitly expressed. Therefore, in this paper, an XY polynomial surface was employed. In order to keep the system axially symmetric, only even order terms of X are retained in the design, and hence the XY polynomial surface is established as an even function of X, expressed as

$$z = \frac{cr^2}{1+\sqrt{1-(1+k)c^2r^2}} + A_{01}x^0y^1 + A_{20}x^2y^0 + A_{02}x^0y^2 + A_{03}x^0y^3 + \cdots + A_{80}x^8y^0. \qquad (18)$$

In the following example, we will see that the aberration performance distribution is X-symmetric in different FOVs.

4. Design Example

As an example, an OTS with SM set as the stop was designed with a focal length of 1200 mm and F-number of 12, and the rectangle FOV of 10° × 4° with $\alpha_1 = 0.455$ and $\alpha_2 = 1.1$ was determined according to the theory above. The initial configuration is shown in Fig. 2.

The modulation transfer function (MTF) of initial configuration is shown in Fig. 3. The wavefront error (WFE) RMS is 0.4095λ ($\lambda = 632.8$ nm). The performance is not good enough as an initial configuration but is acceptable anyway.

The optical system configuration parameters were obtained after further optimization, which was shown in Table 1. In this system, the axial positions of the PM and TM are equal, and both of the PM and TM are with the same radius of curvature and conic. The difference is that the PM adopts the high-order aspheric surface, while the TM adopts the XY polynomial surface. The XY polynomial coefficients are shown in Table 2.

The system imaging optical path is shown in Fig. 4. In the fabrication, the effective part of the PM and TM can be grinded to the same spherical surface on a single substrate, and different high-order aspherical surface and XY polynomial surface will

Table 1. Configuration Parameters

					Aspheric Surface High-Order Term			
	Surface Type	Radius (mm)	Distance (mm)	Conic	6th	8th	10th	Mirror Size (mm)
PM	Even Asphere	−1489.4	−406.8	−1.7402	−6.0274e − 17	6.7990e − 22	−5.2044e − 27	260 × 200
SM	Conic	−624	−406.8	−1.8983				Φ50
TM	XY Polynomial	−1489.4	−600	−1.7402				213 × 145

Table 2. Polynomial Parameters of Freeform TM

No.	Item	Coefficient A_{ij}	No.	Item	Coefficient A_{ij}	No.	Item	Coefficient A_{ij}	No.	Item	Coefficient A_{ij}
1	X^1Y^0	0	10	X^4Y^0	−5.0680e − 011	19	X^1Y^4	0	28	X^7Y^0	0
2	X^0Y^1	3.7014e − 009	11	X^3Y^1	0	20	X^0Y^5	−2.0290e − 013	29	X^6Y^1	−9.1690e − 019
3	X^2Y^0	−1.3710e − 004	12	X^2Y^2	−2.9650e − 010	21	X^6Y^0	6.2147e − 016	30	X^5Y^2	0
4	X^1Y^1	0	13	X^1Y^3	0	22	X^5Y^1	0	31	X^4Y^3	3.9609e − 018
5	X^0Y^2	−1.3790e − 004	14	X^0Y^4	−1.6180e − 010	23	X^4Y^2	1.6520e − 015	32	X^3Y^4	0
6	X^3Y^0	0	15	X^5Y^0	0	24	X^3Y^3	0	33	X^2Y^5	−2.3490e − 017
7	X^2Y^1	−9.1300e − 009	16	X^4Y^1	1.1878e − 013	25	X^2Y^4	−1.0610e − 014	34	X^1Y^6	0
8	X^1Y^2	0	17	X^3Y^2	0	26	X^1Y^5	0	35	X^0Y^7	5.4357e − 018
9	X^0Y^3	−1.5630e − 008	18	X^2Y^3	−2.0540e − 012	27	X^0Y^6	1.5116e − 015	36	X^8Y^0	−3.0140e − 020

be figured at the corresponding parts, which is shown in Fig. 5.

The OTS has a good imaging quality, at the wavelength of 632.8 nm: the MTF is close to the diffraction limit at 50l p/mm (shown in Fig. 6). The maximum WFE RMS is 0.0126λ (shown in Table 3). The distortion grid absolute value is less than 1%, which is shown in Table 4. The RMS radius of image spot is within the Airy spot (the diameter of the Airy disk is 18.528 μm). In particular, it should be noted that because the new XY polynomial that we adopt on TM is established as an even function of x, in the end we achieve an axial symmetrical imaging quality about the x axis that can be proven by the spot diagram shown in Table 5. The axial symmetry aberration performance brings convenience to alignment and testing for OTS, and it makes the alignment of the OTS easier.

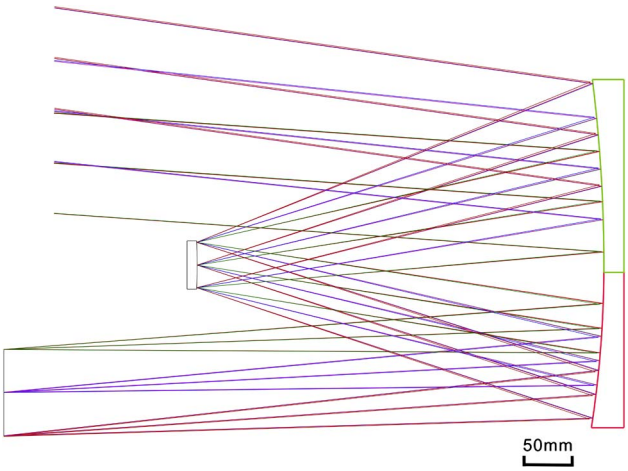

Fig. 4. System imaging optical path.

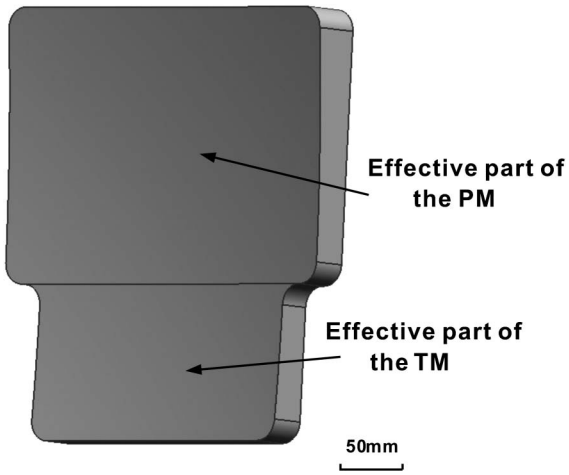

Fig. 5. Effective part of the PM and TM.

5. Tolerance Analysis

The manufacturing and alignment tolerances have been analyzed in the Monte Carlo method; 16 tolerances and compensators have been used, and they are random RMS surface error, radius delta, conic

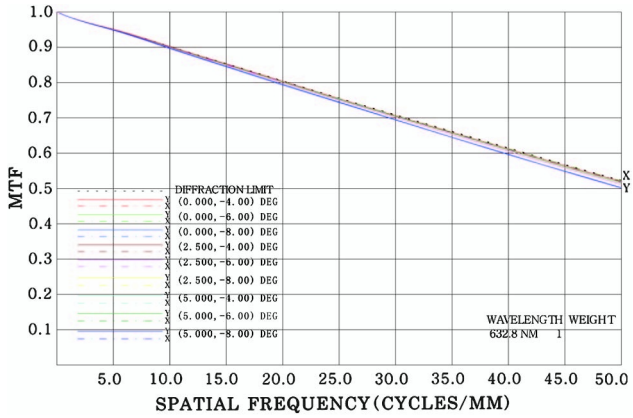

Fig. 6. Modulation transfer function (MTF).

Table 3. WFE (Reference Wave $\lambda = 0.6328$ μm)

FOV	(0°, −4°)	(0°, −6°)	(0°, −8°)	(2.5°, −4°)	(2.5°, −6°)
WFE (RMS)	0.0115λ	0.0084λ	0.0114λ	0.0088λ	0.0127λ
FOV	(2.5°, −8°)	(5°, −4°)	(5°, −6°)	(5°, −8°)	
WFE (RMS)	0.0122λ	0.0109λ	0.0136λ	0.0144λ	

Table 4. Distortion Grid Value

FOV	(0°, −4°)	(0°, −6°)	(0°, −8°)	(2.5°, −4°)	(2.5°, −6°)
Rad. Dist. (%)	−0.19	−0.21	−0.07	−0.2	−0.35
Tan. Dist. (%)	0	0	0	0.1	−0.01
FOV	(2.5°, −8°)	(5°, −4°)	(5°, −6°)	(5°, −8°)	
Rad. Dist. (%)	−0.37	−0.02	−0.44	−0.92	
Tan. Dist. (%)	−0.25	0.34	0.34	0.06	

Table 5. Spot Diagram

(−5°, −4°)	(−2.5°, −4°)	(0°, −4°)	(2.5°, −4°)	(5°, −4°)
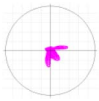		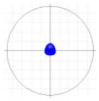		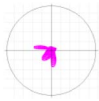
(−5°, −6°)	(−2.5°, −6°)	(0°, −6°)	(2.5°, −6°)	(5°, −6°)
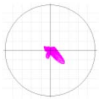		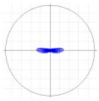		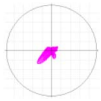
(−5°, −8°)	(−2.5°, −8°)	(0°, −8°)	(2.5°, −8°)	(5°, −8°)
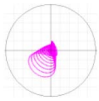		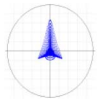		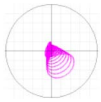

Table 6. Tolerance Value

	Manufacturing Tolerance			Alignment Tolerance	
	Shape error RMS(λ)	Radius (mm)	Conic	Decenter (mm)	Tilt (″)
PM	1/80	±0.75	±0.0005	reference for alignment	
SM	1/80	±0.3	±0.0005	±0.05	±20
TM	1/80	±0.75	±0.0005	reference for alignment	

Table 7. Performance Summary (Polychromatic RMS Wavefront Aberration)

FOV	(0°, −4°)	(0°, −6°)	(0°, −8°)	(2.5°, −4°)	(2.5°, −6°)
Design	0.0115λ	0.0084λ	0.0114λ	0.0088λ	0.0127λ
Design & TOL	0.0720λ	0.0710λ	0.0711λ	0.0713λ	0.0716λ
FOV	(2.5°, −8°)	(5°, −4°)	(5°, −6°)	(5°, −8°)	
Design	0.0122λ	0.0109λ	0.0136λ	0.0144λ	
Design & TOL	0.0714λ	0.0712λ	0.0715λ	0.0715λ	

constant delta, surface x displacement, surface y displacement, and surface tilt (both in tangential and sagittal directions). The thickness between PM (TM) and SM and the back focal length are set as compensators. The tolerance values are shown in Table 6. Noting that SM is set as stop, the surface error of PM and TM are subaperture error. The PM and TM subaperture areas are Φ100 mm and Φ50 mm, respectively, calculated in the footprint plot of CODE V. The performance summary is shown in Table 7. Based on such allocation, this system has a good performance with $\lambda/14(0.0714\lambda)$ WFE.

6. Conclusion

In this paper, we proposed an OTS design that has the PM and TM integrated as a single mirror. It reduces the alignment DOF from 12 to 6 and lowers the alignment difficulty. In addition, the weight and cost of the PM and TM support structures also decrease. In order to increase the design DOF, an XY polynomial freeform surface, with only even order terms of X, is employed, and makes it possible to achieve a wide FOV imaging. The axial-symmetry property of traditional OTS is reserved, which bring convenience to the integration and test. Furthermore, tolerance analysis was carried out, and the final WFE was about $\lambda/14$ while the tolerance values were realizable.

References

1. D. Korsch, "Design and optimization technique for three-mirror telescopes," Appl. Opt. **19**, 3640–3645 (1980).
2. T. Nakano and Y. Tamagawa, "Configuration of an off-axis three-mirror system focused on compactness and brightness," Appl. Opt. **44**, 776–783 (2005).
3. C. Jun, W. Zhicheng, and J. Huiling, "Design on three-reflective-mirror system used in space," Acta Optica Sinica **23**, 216–219 (2003).
4. R. Geyl, "Design and fabrication of a three-mirror, flat-field anastigmat for high-resolution earth observation," Proc. SPIE **2210**, 739–746 (1994).
5. L. D. Mei, Q. X. Geng, and Z. Li, "Optimization design for main supporting structure of the off-axis TMA Space Remote Sensor," in *International Conference on Mechanic Automation and Control Engineering* (IEEE, 2010), pp. 252–254.
6. M. L. Lampton, M. J. Sholl, and M. E. Levi, "Off-axis telescopes for dark energy investigations," Proc. SPIE **7731**,77311G (2010).
7. M. Hartl, H. Mosebach, J. Schubert, H. Michaelis, S. Mottola, E. Kührt, and K. Schindler, "Asteroid finder-the spaceborne

telescope to search for NEO asteroids," in *International Conference on Space Optics* (ESA, 2010), Vol. **4**, p. 8.
8. R. B. Johnson, "Wide field of view three-mirror telescopes having a common optical axis," Opt. Eng. **27**, 121046 (1988).
9. J. Liu, F. Long, and W. Zhang, "Study on computer-aided alignment method of off-axis three-mirror system," Opt. Technol. **5**, 019 (2004).
10. D. Lee, A. Born, P. Parr-Burman, P. Hastings, B. Stobie, and N. Bezawada, "Design of a compact wide field telescope for space situational awareness," Proc. SPIE **8444**, 84440F (2012).
11. Z. Zheng, X. Hao, and X.L Liu, "Freeform surface lens for LED uniform illumination," Appl. Opt. **48**, 6627–6634 (2009).
12. Y. Ding, X. Liu, Z.-R. Zheng, and P.-F. Gu, "Freeform LED lens for uniform illumination," Opt. Express **16**, 12958–12966 (2008).
13. W. Zhang, B. Zuo, S. Chen, H. Xiao, and Z. Fan, "Design of fixed correctors used in conformal optical system based on diffractive optical elements," Appl. Opt. **52**, 461–466 (2013).
14. D. Cheng, Y. Wang, H. Hua, and M. M. Talha, "Design of an optical see-through head-mounted display with a low f-number and large field of view using a freeform prism," Appl. Opt. **48**, 2655–2668 (2009).
15. L. Xu, K. Chen, Q. He, and G. Jin, "Design of freeform mirrors in Czerny-Turner spectrometers to suppress astigmatism," Appl. Opt. **48**, 2871–2879 (2009).
16. P. Junhua, *The Design, Manufacture and Test of the Aspherical Optical Surfaces* (SuZhou University, 2004).
17. V. N. Mahajan, "*Optical Imaging and Aberrations: Part 1. Ray Geometrical Optics* (SPIE, 1998).
18. R. K. Tyson, "Conversion of Zernike aberration coefficients to Seidel and higher-order power-series aberration coefficients," Opt. Lett. **7**, 262–264 (1982).